# Room-temperature oxidation of hypostoichiometric uranium–plutonium mixed oxides $U_{1-y}Pu_yO_{2-x}$ – A depth-selective approach

Romain Vauchy [a, d, e, *], Anne-Charlotte Robisson [a], Renaud C. Belin [a], Philippe M. Martin [a], Andreas C. Scheinost [b, c], Fiqiri Hodaj [d, e]

[a] CEA, DEN, DEC, Cadarache, F-13108 Saint-Paul-lez-Durance, France
[b] Helmholtz Zentrum Dresden-Rossendorf (HZDR), Institute of Resource Ecology, P.O. Box 510119, 01314 Dresden, Germany
[c] Rossendorf Beamline at ESRF, BP 220, F-38043 Grenoble, France
[d] Université de Grenoble Alpes, SIMAP, F-38000 Grenoble, France
[e] CNRS, Grenoble INP, SIMAP, F-38000 Grenoble, France

## ABSTRACT

In the present work, TGA, XAS and XRD were used to evidence the spontaneous oxidation of biphasic $U_{1-y}Pu_yO_{2-x}$ samples, with y = 0.28 and 0.45, at room temperature and upon exposure to low moisture and oxygen contents. The oxidation occurs within very short timescales (*e.g.* O/M ratio increasing from 1.94 to 1.98 within ~1 μm surface layer in ~50 h). The combined use of these three complementary methods offered a depth-selective approach from the sample's bulk to its surface and allowed a thorough understanding of the underlying processes involved during the formation of the oxidized layer and of its thickening with time. We believe our results to be of interest in the prospect of fabricating hypostoichiometric uranium–plutonium mixed oxides since mastering the oxygen content is a crucial point for many of the fuel properties.

© 2015 Elsevier B.V. All rights reserved.

## 1. Introduction

Oxygen stoichiometry in oxide compounds dictates many properties such as thermal/electrical conductivity, melting point and diffusion phenomena [1]. Thus, determining the oxygen stoichiometry is of main interest for various applications, including production of nuclear oxide fuels [2]. In the $UO_2$-$PuO_2$-$Pu_2O_3$ sub-system, $U_{1-y}Pu_yO_{2-x}$ mixed oxides with high plutonium content (>0.20) are multiphasic at room temperature [3–13]. The miscibility gap is composed of two *f.c.c.* phases for the lower Pu contents ($0.20 \leq y \leq 0.45$) and of an *f.c.c.* phase in equilibrium with an α-$Pu_2O_3$-type body centered cubic *b.c.c.* phase in the higher plutonium content range [5–9]. The two phases constituting the hypostoichiometric mixed oxides exhibit different oxygen content and

are then called "high-oxygen" and "low-oxygen" phases, respectively [12,13]. During its lifetime within the nuclear cycle, the fresh uranium–plutonium mixed oxide $U_{1-y}Pu_yO_{2-x}$ is subjected to various atmospheres at room temperature (glove box atmosphere, air, …) for several timespans (*e.g.* storage after sintering). As a consequence, the oxygen to metal ratio (O/M) might be affected, eventually impacting the physical properties of the fuel [14–19]. Thus, a better understanding of the evolution of the oxygen stoichiometry is relevant.

Woodley [20] and Eichler [21] reported a spontaneous oxidation of hypostoichiometric mixed oxides at room temperature by thermogravimetric analysis. They both agree that water chemisorption is responsible for the stoichiometry drift observed in $U_{1-y}Pu_yO_{2-x}$. The oxidation rate of pellets depends on the water vapor concentration, the density of the samples (so their surface area) and the original extent of hypostoichiometry.

According to a model proposed by Guéneau et al. [22] (using the CALPHAD method [23]), if $U_{1-y}Pu_yO_{2-x}$ reaches the

thermodynamic equilibrium during cooling (*e.g.* from 2023 K to room temperature) with the hydrogen-based sintering gas mixture (for instance Ar + 5% $H_2$ + z vpm $H_2O$ with ~5 ≤ z ≤ ~24000), the obtained O/M ratio at room temperature equals 2.000 ± 0.001. A ThermoCalc [24] calculation of the variation in the oxygen potential of iso-O/M compositions in $U_{0.55}Pu_{0.45}O_{2\pm x}$ is shown in Fig. 1 and the two extreme moisture contents in Ar + 5% $H_2$ are represented as dashed lines. Hypostoichiometric uranium–plutonium mixed oxides with high Pu content are then metastable at room temperature even for moisture content in the gas as low as ~5 vpm (*i.e.* an oxidation occurs until attaining O/M ≈ 2).

The current experimental work is focused on realizing an analysis of the extent and kinetics of room-temperature oxidation of hypostoichiometric biphasic uranium–plutonium mixed oxides $U_{1-y}Pu_yO_{2-x}$ samples with y = 0.28 and 0.45. X-ray diffraction, X-ray absorption spectroscopy and gravimetric experiments were performed to study the oxidation process at different scales, *i.e.* surface, grain and bulk, respectively. An illustration of the probing depth of each technique is superimposed with microscopic observations of a $U_{1-y}Pu_yO_2$ pellet (Fig. 2). Concerning the XRD and XAS techniques, it must be taken into account that measurements were performed on powders obtained from crushed pellets and by considering intergranular fracture.

## 2. Experimental

### 2.1. Sample preparation

The uranium dioxide powder was produced by a wet fabrication route based on the formation of ammonium diuranate (ADU) from uranyl nitrate precipitated with ammonia. The obtained particles were then atomized, dried and calcinated, leading to spherical-shaped agglomerates of around 20 μm. Plutonium dioxide powder was produced by precipitation of a plutonium nitrate solution with oxalic acid to form plutonium oxalate. The particles were heated in air at 923 K and parallelepiped-shaped $PuO_2$ particles were obtained with an average size of 15 μm.

Uranium–plutonium mixed oxide samples were obtained by mixing $UO_2$ (72 and 55 mol%, respectively) with $PuO_2$ (28 and 45 mol%, respectively). Each of these two mixtures was then micronized by co-milling in order to increase the U–Pu distribution homogeneity in the final material. Then, each of the powders was pressed into pellets (~2 g/pellet) at ~400 MPa, sintered at 2023 K for 24 h under Ar + 5% $H_2$ + ~1500 vpm $H_2O$ and slowly cooled at ~0.01 K s⁻¹. These conditions were determined according to the thermodynamic model proposed by Lindemer and Besmann [25–27] to obtain stoichiometric compounds (x = 0). The obtained pellets were free from defects with a high density (>95% of the theoretical density). The average grain size was determined by observing the microstructure of polished dense pellets after chemical etching and was equal to 30–40 μm regardless of the Pu content (Fig. 3).

The detailed fabrication process is described elsewhere [28]. The pellets were annealed at 2023 K for 4 h under Ar + 5% $H_2$ + ~5 vpm $H_2O$ and cooled as fast as possible in the considered furnace (~0.08 K s⁻¹) in order to obtain biphasic hypostoichiometric mixed oxides (*i.e.* to limit their oxidation during cooling). As shown in a previous study, the kinetics of phase separation is very rapid regardless of the cooling rate from 0.05 to 300 K s⁻¹ [12,13]. Prior to measurement, the XRD samples were reduced *in situ* in the high-temperature diffractometer and subsequently analyzed. The resulting hypostoichiometric samples annealed in the furnace and in the HT-XRD are then noted "$U_{1-y}Pu_yO_{2-x}$".

The regular glove-box atmosphere used in our laboratory, which is composed of $N_2$ + ~30 vpm $O_2$ + ~50 vpm $H_2O$, was the oxidation

media for all the characterization techniques. Reconstituted air ($N_2$ + 21% $O_2$ + ~5 vpm $H_2O$) was also used for XRD measurements performed on $U_{0.55}Pu_{0.45}O_{2-x}$. The $H_2O$ and $O_2$ contents were measured with a capacitive Vaisala DM70 probe and a Systech 600 oxygen sensor, respectively. The two atmospheres exhibiting oxygen and moisture concentrations different by a factor of 7000 and 10, respectively, the surface-oxidation rates were determined to show the influence of $O_2$ and $H_2O$ in the oxidation mechanism.

### 2.2. Apparatus and experimental techniques

Bulk-scale O/M ratio measurements were performed by gravimetric method using an ADAMEL furnace coupled with a gas-mixing device allowing the control of the atmosphere, and more precisely, its oxygen partial pressure $pO_2$ as a function of temperature. Oxygen partial pressures were controlled *via* the moisture content of an Ar + 5% $H_2$ gas mixture and set by diverting a fraction of the Ar/$H_2$ flow through water maintained at 288 K and measured, at room-temperature, with a capacitive probe. A special SETNAG yttria-stabilized zirconia oxygen probe was placed in the furnace in order to measure *in situ* the oxygen partial pressure of the gas in equilibrium with the samples. A reference $pO_2$ was set using an intimate solid mixture of Ir/$IrO_2$. The measured and calculated oxygen partial pressures were, in all cases, in very good agreement and the deviation was less than 1/10 of the target value. Thermal treatments at 1173 K for 24 h under Ar + 5% $H_2$ + ~24000 vpm $H_2O$ were applied to the hypostoichiometric mixed oxide pellets. According to the Guéneau's model [22], these thermodynamic conditions lead to stoichiometric samples (O/M = 2.000 ± 0.001), see also Fig. 1. The resulting mixed oxides are then noted "$U_{1-y}Pu_yO_{2.000}$" as compared to the initial hypostoichiometric $U_{1-y}Pu_yO_{2-x}$ samples. By comparing the initial pellet's mass to the one after the thermal treatment and by considering the final stoichiometry being 2.000, the initial O/M ratio can be calculated with the Eq. (1) with an accuracy of ±0.001. This excellent accuracy was obtained by taking into account the repeatability of the experiment with other pellets of the same batch and the stoichiometry was checked again with a NETZSCH Jupiter STA 449C thermobalance coupled to a similar moisture control device.

$$\frac{O}{M} = 2\pm x = 2\pm\frac{M_{U_{1-y}Pu_yO_2}}{M_O}\cdot\frac{|m_f - m_i|}{m_f} \qquad (1)$$

With:

$\frac{O}{M}$: initial oxygen-to-metal ratio of $U_{1-y}Pu_yO_{2\pm x}$
$x$: deviation from stoichiometry
$M_{U_{1-y}Pu_yO_2}$: molar mass (g mol⁻¹) of $U_{1-y}Pu_yO_{2.000}$ (taking into account the isotopic composition of uranium and plutonium)
$M_O$: molar mass of oxygen
$m_f$: mass of $U_{1-y}Pu_yO_{2.000}$
$m_i$: initial mass of $U_{1-y}Pu_yO_{2\pm x}$

As illustrated in Fig. 4, mass variations of a hypostoichiometric mixed oxide pellet (initially ~2 g) were still observed when decreasing temperature between 1523 and 1373 K under Ar + 5% $H_2$ + 200 vpm $H_2O$. This shows that smaller deviations from stoichiometry are still measurable within this range. However, in order to provide reasonable O/M ratio values, an uncertainty of ±0.001 on their determination was considered. Furthermore, according to Fig. 1, the mass leading to O/M = 2.000 ± 0.001 is reached, for $U_{0.55}Pu_{0.45}O_{2\pm x}$, at 1473 K at equilibrium. Thus, treating the samples at lower temperatures, longer durations and higher moisture contents increases the chance to reach O/M = 2.000 ± 0.001 and to
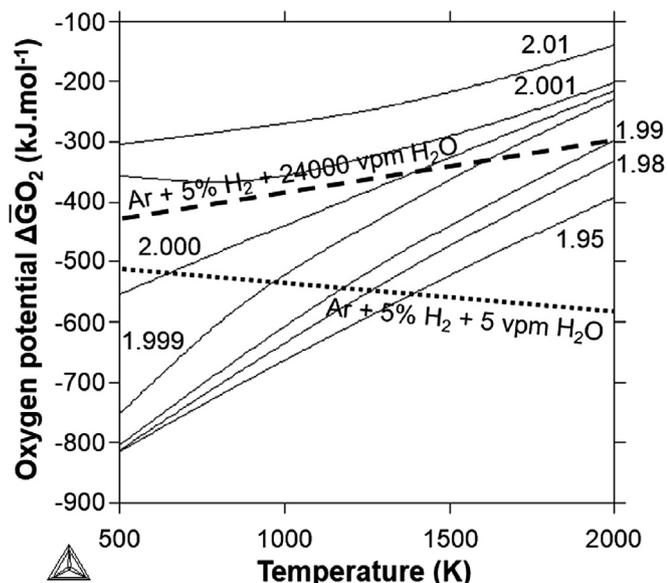
**Fig. 1.** Variation in the oxygen potential of iso-O/M ratio compositions in $U_{0.55}Pu_{0.45}O_{2\pm x}$ as a function of temperature [24].

measure the oxygen stoichiometry with an accuracy of $\pm 0.001$.

XAS measurements were performed at the Rossendorf Beamline (BM20) located at the European Synchrotron Radiation Facility (ESRF, Grenoble, France). Storage ring operating conditions were 6.0 GeV and 170—200 mA. A double crystal monochromator

mounted with Si (111) crystals was used.

XAS samples were prepared by mixing about 1 mg of material (obtained by manually crushing a dense pellet) with 20 mg of boron nitride. Samples were then pressed into a thin bar to match the dimension of the illuminating X-ray beam while minimizing the amount of sample required. The pellet was then inserted into a hermetic Teflon container, and in addition into a sealed poly-ethylene sample holder to provide a double confinement to fulfill radioprotection requirements of the synchrotron facility. Mea-surements were carried out at room temperature [29].

XANES spectra were collected in transmission mode at $U-L_{III}$ (17166 eV) and $Pu-L_{III}$ (18057 eV) edges. Y (17038 eV) and Zr (17998 eV) foils were located between the second and the third ionization chamber for energy calibration. The ATHENA software [30] was used for normalizing XANES spectra. The $E_0$ values were taken at the first inflexion point using the first zero-crossing value of the second derivative. The position of white line maximum was determined by the first zero-crossing of the first derivative. $UO_2$, $U_4O_9$, $U_3O_8$, $PuO_2$ and $PuF_3$ were used as references for the oxida-tion states of the uranium [29,31,32] and plutonium [29,33—35] cations, respectively. Although the empty density of state probed by XANES is different between $PuF_3$ and plutonium oxides, the core-hole lifetime (8.7 eV) at $Pu-L_{III}$ edge is too large to observe such slight modifications in the collected XANES spectra. As an illustration, a previous study shown that $PuF_3$ results are identical to those obtained for (U(IV),Pu(III)) mixed oxalates [35]. The latter being a similar system to that of the current study, the use of $PuF_3$ as the Pu(III) reference is thus adequate. Experimental XANES data were fitted between $-20$ and $+30$ eV compared to the $E_0$ position.
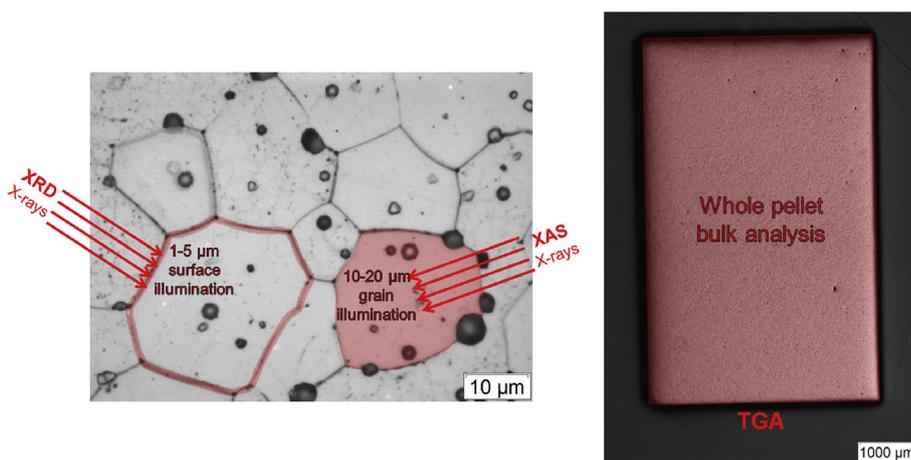


**Fig. 2.** Illustration of probed depths with XRD, XAS and TGA in $U_{1-y}Pu_yO_2$.



$U_{0.72}Pu_{0.28}O_2$

$U_{0.55}Pu_{0.45}O_2$
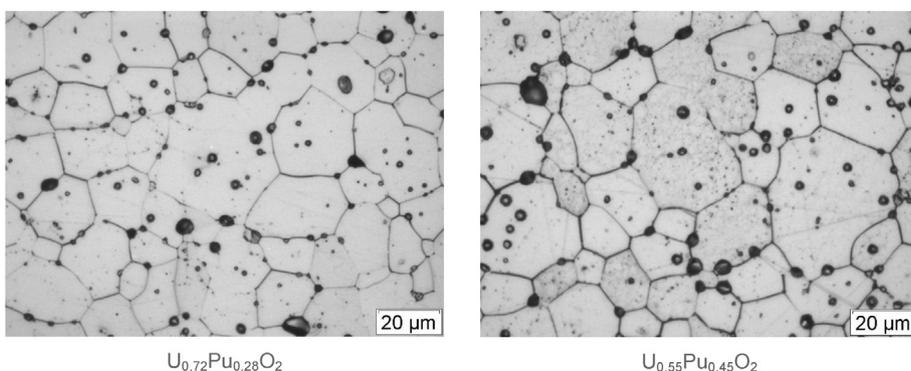
**Fig. 3.** Microstructures (x50) after chemical etching of $U_{1-y}Pu_yO_2$ mixed oxides.
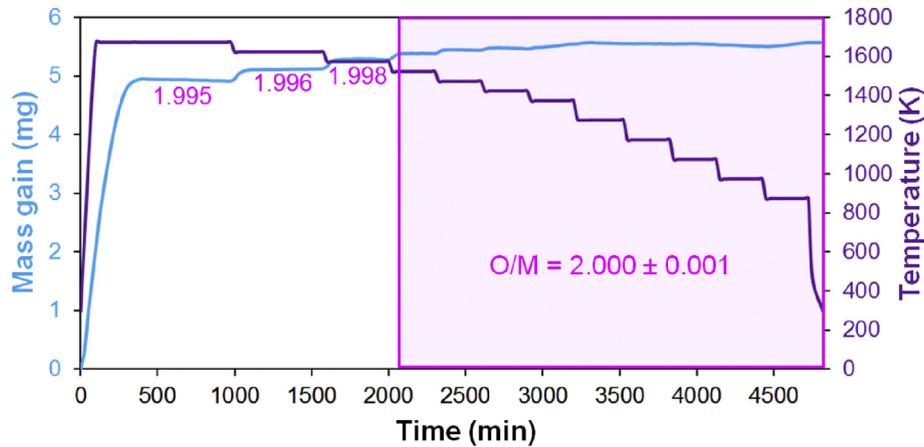
**Fig. 4.** Re-oxidizing thermal treatment of $U_{0.72}Pu_{0.28}O_{2-x}$ under Ar + 5% $H_2$ + 200 vpm $H_2O$ showing the accuracy of the TGA analysis.

**Table 1**
Gravimetric results of room-temperature oxidation of $U_{1-y}Pu_yO_{2-x}$ pellets under glove-box atmosphere.

|  | Measured $(O/M)_{total}$ ratio[a] | |
|---|---|---|
| y = Pu/(U + Pu) | 0.28 | 0.45 |
| $t_0$ | 1.942 ± 0.001 | 1.927 ± 0.001 |
| $t_0$ + 3 months | 1.950 ± 0.001 | 1.938 ± 0.001 |
| $t_0$ + 9 months | – | 1.976 ± 0.001 |
| $t_0$ + 17 months | 1.954 ± 0.001 | – |

[a] $(O/M)_{total}$ values are average ones calculated by assuming constant the O/M ratio all over the sample.

The goodness of the fit is estimated with both $R$ factor and $\chi^2$ values.

Only the XANES part of the spectra were used in this study because the target was here to determine the cation oxidation states giving the overall O/M ratio (±0.01) by linear combination of the whole XANES spectra of reference species (*e.g.* Pu(III) and Pu(IV)).

All XRD measurements were performed at atmospheric pressure and room temperature with a Bragg–Brentano θ–θ Bruker D8 Advance X-ray diffractometer using copper radiation from a conventional tube source (Kα$_1$ + Kα$_2$ radiation: λ = 1.5406 and 1.5444 Å) at 40 kV and 40 mA on dense pellets manually crushed. The entire apparatus resides in its own custom-built nitrogen-filled

glove-box dedicated to handling of actinides compounds at the LEFCA facility (CEA Cadarache, France). Further technical details and data refinement methods (lattice parameters obtained by Pawley refinement [36] and phase fractions by the Rietveld analysis [37]) are reported elsewhere [12,38].

Considering the lattice parameters, it is possible to calculate the individual O/M (=2−x) ratio (±0.003) of each phase at room temperature with an empirical correlation connecting the lattice parameter, the plutonium content and the deviation from stoichiometry (2) deduced from Duriez et al. [15], also consistent with Ohmichi et al. [39].

$$a = 547 - 7.4y + 32x \tag{2}$$

With:

*a*: lattice parameter (pm)
*y*: plutonium content (Pu/(U + Pu))
*x*: deviation from stoichiometry

As confirmed by Electron Probe Micro-Analysis (EPMA) experiments performed on the two biphasic mixed oxides (y = 0.28 and 0.45), the plutonium content of the low- and high-oxygen phases of each mixed oxide are identical at room temperature.

The overall O/M ratio was then calculated using an approach
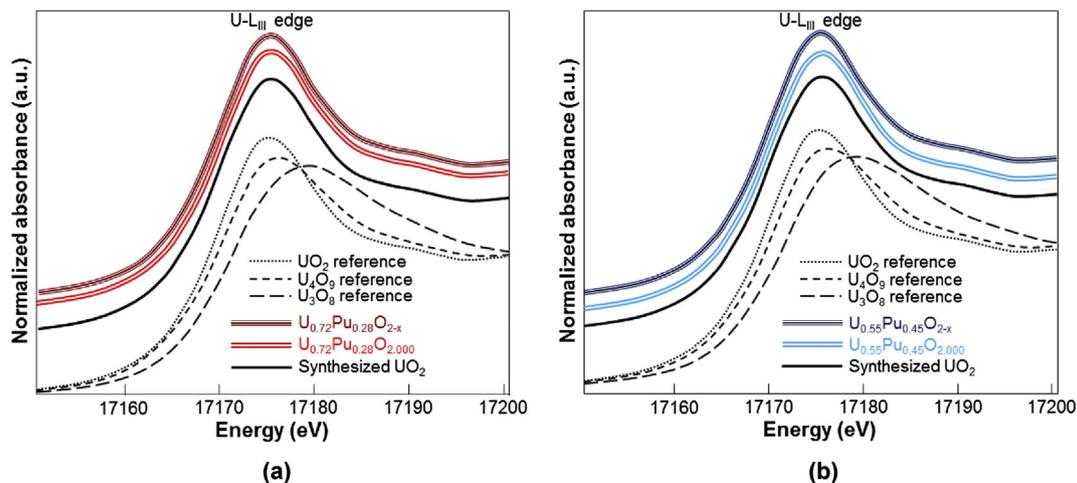


**Fig. 5.** XANES spectra collected in transmission mode at U-L$_{III}$ edge for samples after reducing annealing $U_{1-y}Pu_yO_{2-x}$ and after oxidizing thermal treatment $U_{1-y}Pu_yO_{2.000}$ with (a) y = 0.28 and (b) y = 0.45. Spectra are compared with uranium oxide references (thin dashed lines).
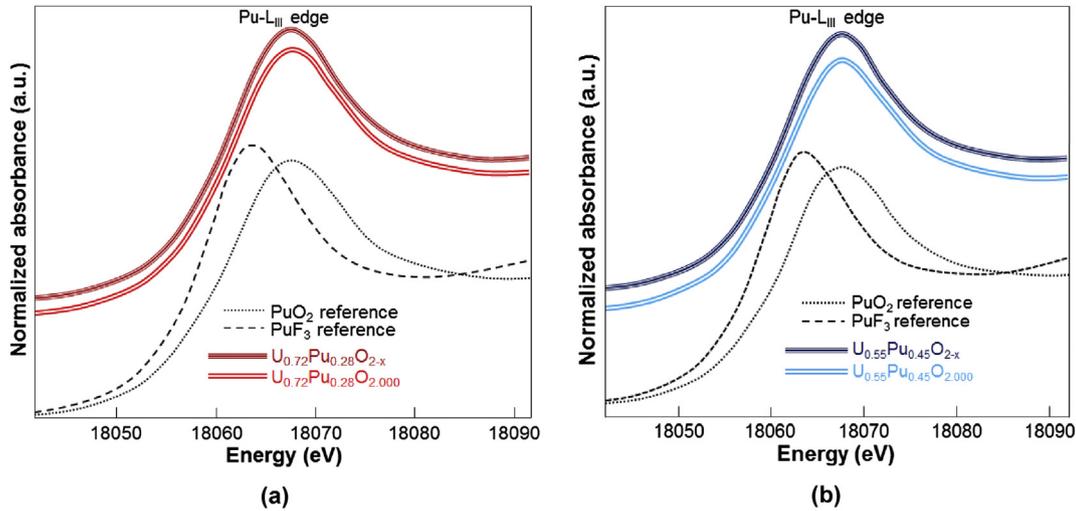
**Fig. 6.** XANES spectra collected in transmission mode at Pu-L$_{III}$ edge for samples after reducing annealing U$_{1-y}$Pu$_y$O$_{2-x}$ and after oxidizing thermal treatment U$_{1-y}$Pu$_y$O$_{2.000}$ with (a) y = 0.28 and (b) y = 0.45. Spectra are compared with Pu(IV) and Pu(III) references (thin dashed lines).

**Table 2**
XANES results and (O/M)$_{total}$ ratio calculations.

| Sample | Edge | | | | | | | | | O/M ratio |
|---|---|---|---|---|---|---|---|---|---|---|
| | U-L$_{III}$ | | | | | Pu-L$_{III}$ | | | | |
| | $E_0$ (eV) | White line maximum (eV) | wt.% UO$_2$ | wt.% U$_4$O$_9$ | wt.% U$_3$O$_8$ | $E_0$ (eV) | White line maximum (eV) | wt.% PuF$_3$ | wt.% PuO$_2$ | |
| U$_{0.72}$Pu$_{0.28}$O$_{2-x}$ | 17170.3 | 17175.6 | 100 | 0 | 0 | 18061.9 | 18067.5 | 0 | 100 | 2.00 ± 0.01 |
| U$_{0.55}$Pu$_{0.45}$O$_{2-x}$ | 17170.5 | 17175.8 | 96 ± 2 | 4 ± 2 | 0 | 18062.0 | 18067.8 | 0 | 100 | 2.01 ± 0.01 |
| Synthesized UO$_2$ | 17170.7 | 17175.7 | 96 ± 2 | 4 ± 2 | 0 | – | – | – | – | 2.01 ± 0.01 |
| U$_{0.72}$Pu$_{0.28}$O$_{2.000}$ | 17170.3 | 17175.6 | 100 | 0 | 0 | 18062.0 | 18067.7 | 0 | 100 | 2.00 ± 0.01 |
| U$_{0.55}$Pu$_{0.45}$O$_{2.000}$ | 17170.7 | 17175.8 | 94 ± 2 | 6 ± 2 | 0 | 18062.1 | 18067.8 | 0 | 100 | 2.01 ± 0.01 |
| Synthesized UO$_2$ | 17170.7 | 17175.7 | 97 ± 2 | 3 ± 2 | 0 | – | – | – | – | 2.00 ± 0.01 |

similar to that given by Verma and Roy [40] by considering the O/M ratio of each phase and its respective fraction obtained by Rietveld refinement [37] (3).

$$\left(\frac{O}{M}\right)_{global} = f_{\varphi_1} \cdot \left(\frac{O}{M}\right)_{\varphi_1} + f_{\varphi_2} \cdot \left(\frac{O}{M}\right)_{\varphi_2} \qquad (3)$$

With:

$f_{\varphi_n}$: n-phase fraction as determined by Rietveld refinement
$\left(\frac{O}{M}\right)_{\varphi_n}$: n-phase O/M ratio of the as determined by (2)

The associated oxidation rates were finally calculated with (4).

$$\tau = \frac{\partial(O/M)}{\partial t} \qquad (4)$$

With:

$\tau$: oxidation rate (h$^{-1}$)
$t$: time (h)

## 3. Results and discussion

### 3.1. Evidence for room-temperature oxidation at the scale of the pellet

Gravimetric O/M ratio measurements were performed on ~2 g

dense pellets (d > 95% d$_{th}$) directly after annealing under reducing conditions, referenced as $t_0$, and compared with the same samples stored for various durations (up to 17 months) under the glove-box atmosphere (N$_2$ + ~30 vpm O$_2$ + ~50 vpm H$_2$O). Results for both y = 0.28 and 0.45 mixed oxides are shown in Table 1.

The significant increase in the (O/M)$_{total}$ values clearly indicates that oxidation appeared to be significant at the scale of the pellet despite the fact that it was subjected to an apparently inert atmosphere for few months. Furthermore, the U$_{0.55}$Pu$_{0.45}$O$_{2-x}$ mixed oxide being more reduced than the U$_{0.72}$Pu$_{0.28}$O$_{2-x}$ one, its oxidation was slightly faster which is consistent with the observations of Woodley [20] concerning the extent of hypostoichiometry.

### 3.2. Evidence for room-temperature oxidation at the scale of the grain

In order to better understand the spontaneous oxidation phenomenon occurring at room-temperature in U$_{1-y}$Pu$_y$O$_{2-x}$, X-ray absorption spectroscopy experiments were performed. XAS using high energy light source generated with a synchrotron, the probed depth in U$_{1-y}$Pu$_y$O$_{2-x}$ compounds is equal to tens of microns [35]. The grain size of the fabricated samples being of the same scale as the synchrotron X-rays probing depth, the whole grains were then illuminated by the X-ray source. The XAS experiment was performed on both hypostoichiometric samples stored in the glove-box for 3 months and thermally re-oxidized compounds (at 1173 K for 24 h under Ar + 5% H$_2$ + ~24000 vpm H$_2$O) in order to

hypothetically reveal a stoichiometry difference between the samples.

Normalized spectra at U-$L_{III}$ edge collected on both reduced ($U_{1-y}Pu_yO_{2-x}$) and after oxidizing thermal treatment ($U_{1-y}Pu_yO_{2.000}$) are compared with reference compounds ($UO_2$, $U_4O_9$ and $U_3O_8$) and shown in Fig. 5. All the XANES spectra were perfectly aligned on the $UO_2$ reference demonstrating that all uranium cations were tetravalent.

The XANES spectra of plutonium were also collected on the same samples at Pu-$L_{III}$ edge. The normalized spectra compared with Pu(IV)$O_2$ and Pu(III)$F_3$ references are shown in Fig. 6. If we consider the compounds with y = 0.28 (Fig. 6(a)) and y = 0.45 (Fig. 6(b)) after thermal treatment leading to stoichiometric ($U_{1-y}Pu_yO_{2.000}$) mixed oxides, all the plutonium contained in these samples was tetravalent because the associated XANES spectra were perfectly aligned with the one relative to the $PuO_2$ reference. When considering the reducing conditions, all the mixed oxides were again aligned with the $PuO_2$ reference *i.e.* exhibited an O/M ratio equal to 2.00 and then evidenced a clear oxidation phenomenon at the scale of the grain occurring during storage in the glove-box at room-temperature between the reducing annealing and the XAS analysis.

The results refined with the ATHENA Software [30] are shown in Table 2. The O/M ratio calculations were performed by connecting the oxidation state of each cation and its concentration in the analyzed compounds.

The results listed in Table 2 clearly evidence a room-temperature oxidation phenomenon occurring in the hypo-stoichiometric mixed oxides. Despite the great care taken to limit exposure to the glove-box atmosphere when preparing the XAS samples, the experiment did not reveal a difference in the O/M ratio values. Because hard X-rays penetrates up to tens of microns in the mixed oxide [35] which matches the grain size (30–40 μm), it can be deduced that spontaneous oxidation was neither avoided nor limited to the surface of the grains but propagated through the whole grains.

### 3.3. Evidence for room-temperature oxidation at the scale of the surface of the grain

In order to discriminate the process taking place at the grain surface from that in the bulk structure, we applied XRD measurements on both raw and abraded $U_{0.55}Pu_{0.45}O_{2-x}$ dense pellets, two days after annealing at 2023 K for 4 h under Ar + 5% $H_2$ + ~5 vpm $H_2O$. The X-rays generated by the XRD device penetrating only in a thin layer (roughly 1 μm) in the uranium−plutonium mixed oxides,
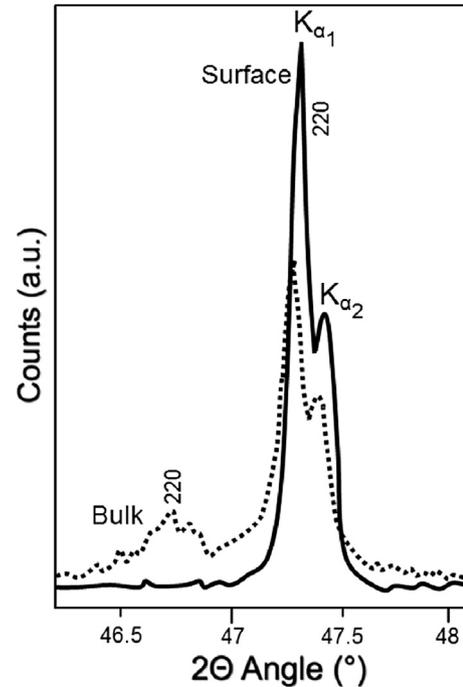
Fig. 7. (220) peaks of the *f.c.c.* structure collected on a $U_{0.55}Pu_{0.45}O_{2-x}$ pellet 48 h after reducing annealing, surface and bulk (before and after abrasion) are shown in solid and dashed lines, respectively.
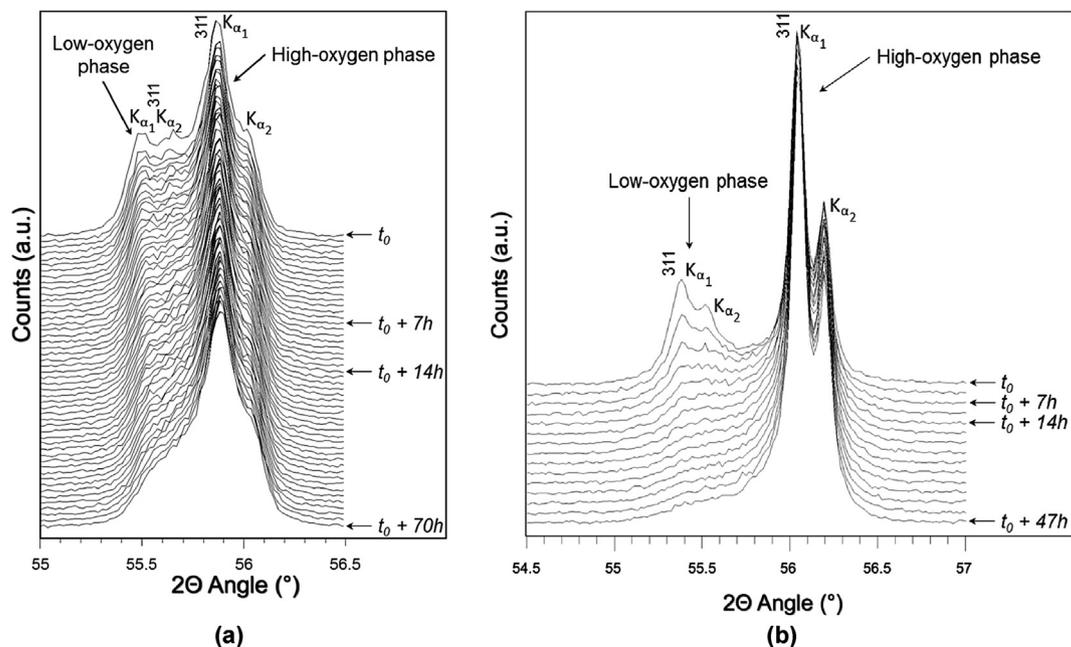
Fig. 8. (311) peaks of the 2× *f.c.c.* structures of (a) $U_{0.72}Pu_{0.28}O_{2-x}$ and (b) $U_{0.55}Pu_{0.45}O_{2-x}$ subjected at room-temperature to the glove-box atmosphere.
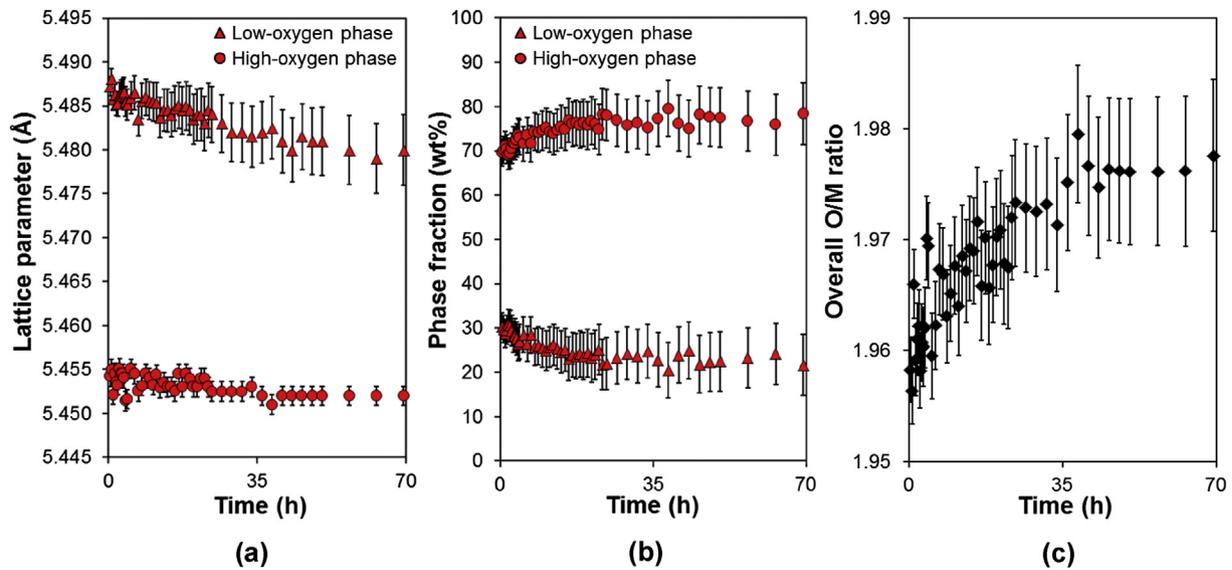
**Fig. 9.** Evolution at room temperature under $N_2$ + ~30 vpm $O_2$ + ~50 vpm $H_2O$ of (a) lattice parameters, (b) phase fractions and (c) overall O/M ratio of $U_{0.72}Pu_{0.28}O_{2-x}$.
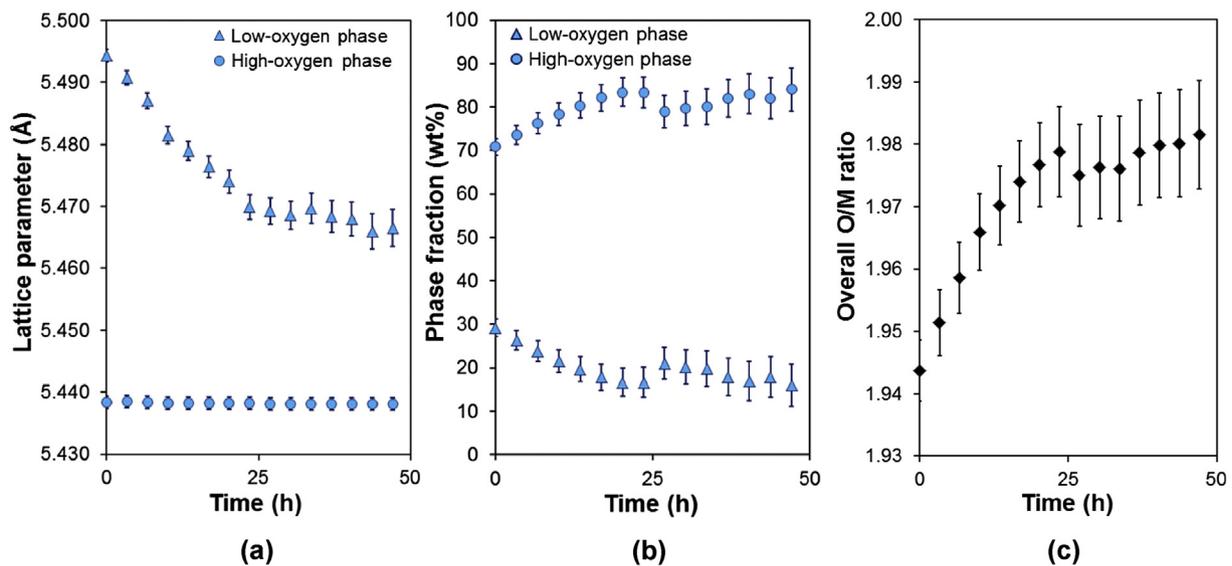


**Fig. 10.** Evolution at room temperature under $N_2$ + ~30 vpm $O_2$ + ~50 vpm $H_2O$ of (a) lattice parameters, (b) phase fractions and (c) overall O/M ratio of $U_{0.55}Pu_{0.45}O_{2-x}$.

the spontaneous room-temperature oxidation was detected only at the surface of the grains. As shown in Fig. 7, the evolution of the (220) peak of the *f.c.c.* structure revealed a monophasic stoichiometric composition for the raw surface (solid line) and a biphasic reduced bulk (dashed line). This experiment evidenced the fast kinetics the surface oxidation of the grains taking place in $U_{1-y}Pu_yO_{2-x}$ compounds subjected to the glove-box atmosphere.

### 3.3.1. Oxidation of $U_{0.72}Pu_{0.28}O_{2-x}$ and $U_{0.55}Pu_{0.45}O_{2-x}$ under glove-box atmosphere

The evolution of the (311) peaks of both samples as a function of time is shown in Fig. 8 and the obtained lattice parameters, phase fractions and overall O/M ratio are shown in Fig. 9 and Fig. 10 for $U_{0.72}Pu_{0.28}O_{2-x}$ and $U_{0.55}Pu_{0.45}O_{2-x}$, respectively. X-ray patterns were collected for 70 h and 47 h on the y = 0.28 and 0.45 mixed oxides, respectively. In both cases, the peak of the low-oxygen phase (located at lower angle) was shifted to higher angles with

time because of a lattice contraction induced by a changing in chemical composition resulting from oxidation. The lattice parameter of the low-oxygen phase of $U_{0.72}Pu_{0.28}O_{2-x}$ shifted to higher angles more slowly than that of $U_{0.55}Pu_{0.45}O_{2-x}$. These two low-oxygen phases exhibiting at $t_0$ an O/M ratio equal to 1.881 ± 0.003 and 1.819 ± 0.003 (Eq. (2) with O/M = 2−x), respectively, this observation is somehow consistent with the results given by Woodley [20] *i.e.* that the oxidation rate depends on the extent of hypostoichiometry.

Furthermore, in both cases, the intensity of the diffraction peaks of the reduced phases significantly decreased as a function of time. Again, the low-oxygen phase of the samples with y = 0.28 disappeared more slowly than that with y = 0.45.

This decrease in intensity coupled to the declining in the lattice parameter of the low O/M ratio phase both evidenced the surface oxidation phenomenon occurring in the hypostoichiometric samples at a relatively short timescale.
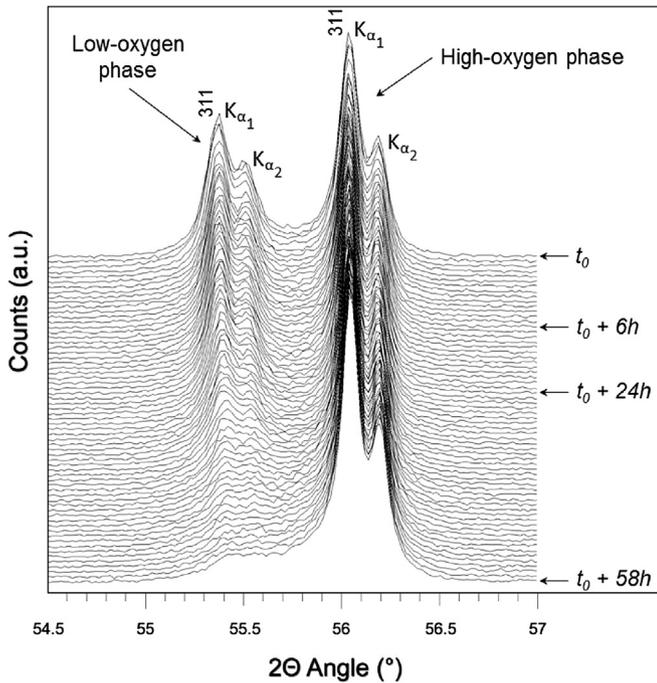
**Fig. 11.** (311) peaks of the 2× *f.c.c.* structures of $U_{0.55}Pu_{0.45}O_{2-x}$ subjected to reconstituted air at room-temperature.

As shown in Figs. 9(b) and 10(b), the overall O/M ratio of the two samples promptly increased within the first 20 h and, in both cases, stabilized around a value of 1.98 corresponding to the upper limit of the miscibility gap existing in the $UO_2$-$PuO_2$-$Pu_2O_3$ sub-system [8].

### 3.3.2. Oxidation of $U_{0.55}Pu_{0.45}O_{2-x}$ under reconstituted air

The diffraction patterns at room-temperature focused on the (311) peaks of the two *f.c.c.* structures constituting the $U_{0.55}Pu_{0.45}O_{2-x}$ sample are shown in Fig. 11. As for the samples oxidized at room temperature under the glove-box atmosphere, the diffraction peaks of the low-oxygen phase of $U_{0.55}Pu_{0.45}O_{2-x}$ sample decreased as a function of time. Its lattice parameter also
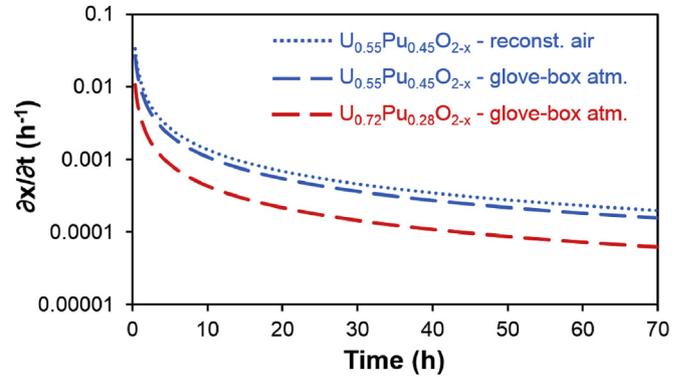


**Fig. 13.** Oxidation rates of $U_{0.72}Pu_{0.28}O_{2-x}$ and $U_{0.55}Pu_{0.45}O_{2-x}$ samples as a function of the time and the atmosphere.

changed and tended to reach that of the high-oxygen phase. The evolution of the lattice parameters and of the phase fractions as a function of time are shown in Fig. 12. The oxidation rate of the low-oxygen phase was here slightly slower than under the glove-box atmosphere (Fig. 10(a)). After 24 h, the lattice parameter of the low-oxygen phase under the glove-box atmosphere was equal to 5.470 ± 0.001 Å compared to 5.482 ± 0.001 Å under air. This difference might be explained by the one order of magnitude difference in moisture content between the glove-box atmosphere and reconstituted air. Again, the overall O/M ratio of the sample rapidly increased within the first 20 h and stabilized at around 1.98.

According to these data, the oxidation rates of the samples subjected to either glove-box atmosphere or reconstituted air were calculated and the associated tendencies are reported in Fig. 13.

The general trend was similar for the two $U_{0.55}Pu_{0.45}O_{2-x}$ samples regardless of the atmosphere even if the oxidation rate under the glove-box atmosphere was, to some extent, higher. The moisture content differing only by a factor of 10 (as compared to 7000 for oxygen content), the room-temperature oxidation of $U_{1-y}Pu_yO_{2-x}$ appeared to be mainly governed by the moisture content of the gas. These observations are in agreement with the literature [20,21]. Fig. 14 proposes a tentative oxidation mechanism of hypostoichiometric uranium–plutonium mixed oxides $U_{1-y}Pu_yO_{2-x}$ based on moisture reactivity with oxygen vacancies
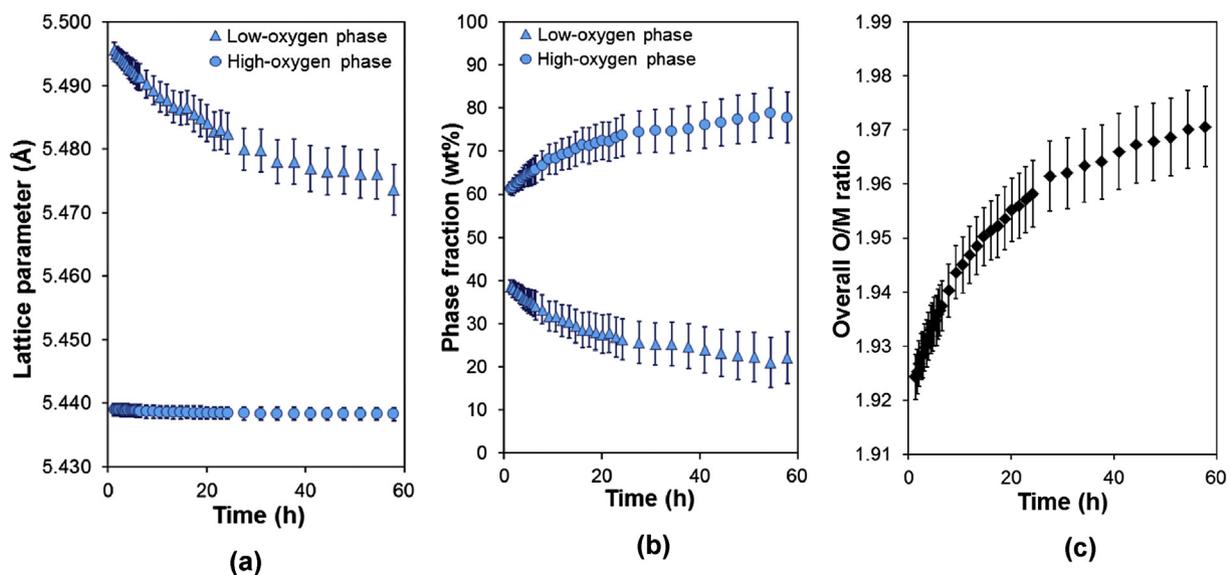


**Fig. 12.** Evolution at room temperature under $N_2$ + 21% $O_2$ + ~5 vpm $H_2O$ of (a) lattice parameters, (b) phase fractions and (c) overall O/M ratio of $U_{0.55}Pu_{0.45}O_{2-x}$.
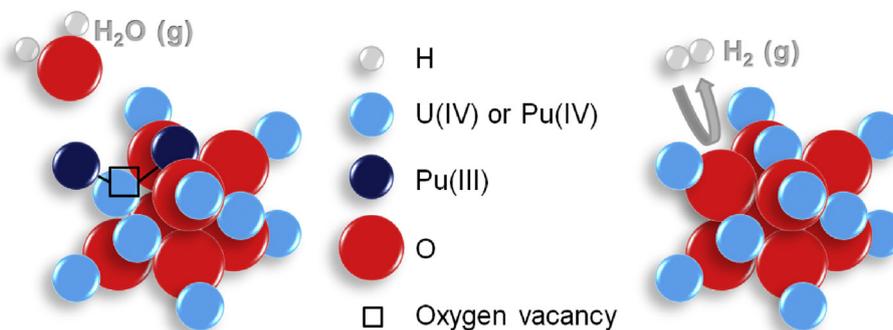
**Fig. 14.** Suggested room-temperature oxidation mechanism of $U_{1-y}Pu_yO_{2-x}$.

leading to $H_2$ (g) release which was recorded in Refs. [20,21].

Furthermore, the plutonium content, which directly drives the extent of hypostoichiometry [14], has a clear influence on this oxidation rate. $U_{0.72}Pu_{0.28}O_{2-x}$ is thus oxidized at a lower rate than $U_{0.55}Pu_{0.45}O_{2-x}$. Samples with less Pu are less hypostoichiometric and therefore the time needed to reach the O/M = 2.000 stoichiometry will be longer [20,21].

## 4. Conclusion

By coupling gravimetric measurements, X-ray absorption spectroscopy and X-ray diffraction, we report the occurrence of spontaneous room-temperature oxidation of hypostoichiometric uranium–plutonium $U_{1-y}Pu_yO_{2-x}$ mixed oxides with y = 0.28 and 0.45 at three different depths (from the scale of the pellet to the surface of the grains). This spontaneous oxidation of biphasic $U_{1-y}Pu_yO_{2-x}$ samples subjected to very low oxygen and moisture contents (*e.g.* glove-box atmosphere) was evidenced to be a surface process. Furthermore, the change in stoichiometry is influenced by the moisture content of the atmosphere rather than by its oxygen concentration inducing that oxidation mechanism at room-temperature is driven by water chemisorption. The oxidation phenomenon is governed by the variation in stoichiometry of the low-oxygen phase, *i.e.* change in its lattice parameter, coupled to the decrease in its fraction. Furthermore, both extent and kinetics of the oxidation phenomenon dictate a cautious attitude when fabricating and/or handling hypostoichiometric uranium–plutonium mixed oxides with a high plutonium content.

With respect to the analytical methods employed, this depth-selective study also points out clear differences between the various ways of determining the O/M ratio of $U_{1-y}Pu_yO_{2-x}$. This suggests choosing the appropriate experimental technique for determining the deviation from stoichiometry in $U_{1-y}Pu_yO_{2-x}$ or more generally in hypostoichiometric oxides.

## References

[1] O.T. Sørensen, Nonstoichiometric oxides, Mater. Sci. Ser. (1981) 1–59.
[2] A Technology Roadmap for the Generation IV Nuclear Energy Systems, US Department of Energy Nuclear Energy Research Advisory Committee and the Generation IV International Forum, December 2002.
[3] L.E. Russell, N.H. Brett, J.D.L. Harrison, J. Williams, J. Nucl. Mater. 5 (1962) 216–227.
[4] N.H. Brett, L.E. Russell, Trans. Brit. Ceram. Soc. 62 (1962) 97–118.
[5] T.L. Markin, R.S. Street, Inorg. Nucl. Chem. 29 (1967) 2265–2280.
[6] T.L. Markin, E.J. McIver, Plutonium 1965, Chapman and Hall, London, 1967, pp. 845–857.
[7] C. Sari, U. Benedict, H. Blank, Thermo. Nucl. Mater (1968) 587–611.
[8] C. Sari, U. Benedict, H. Blank, J. Nucl. Mater. 35 (1970) 267–277.
[9] G. Dean, J.C. Boivineau, P. Chereau, J.P. Marcon, Plutonium and Other Actinides, Plutonium 1970, 1970, pp. 753–761.
[10] T. Truphémus, R.C. Belin, J.C. Richaud, J. Rogez, Proc. Chem. 7 (2012) 521–527.
[11] T. Truphémus, R.C. Belin, J.C. Richaud, M. Reynaud, M.A. Martinez, I. Félines, A. Arredondo, A. Miard, T. Dubois, F. Adenot, J. Rogez, J. Nucl. Mater. 432 (2013) 378–387.
[12] R. Vauchy, R.C. Belin, A.C. Robisson, F. Hodaj, J. Eur. Ceram. Soc. 30 (10) (2014) 2543–2551.
[13] R. Vauchy, R.C. Belin, A.C. Robisson, F. Hodaj, M.R.S. Proc. Mater. Res. Soc. 2014 (2013) 1645.
[14] M. Beauvy, J. Nucl. Mater. 188 (1992) 232–238.
[15] C. Duriez, J.P. Alessandri, T. Gervais, Y. Philipponneau, J. Nucl. Mater. 277 (2000) 143–158.
[16] M. Inoue, J. Nucl. Mater. 282 (2000) 186–195.
[17] P.R. Vasudeva Rao, S. Anthonysamy, M.V. Krishnaiah, V. Chandramouli, J. Nucl. Mater. 348 (2006) 329–334.
[18] K. Morimoto, M. Kato, H. Uno, A. Hanari, T. Tamura, H. Sugata, T. Sunaoshi, S. Kono, J. Phy. Chem. Sol. 66 (2005) 634–638.
[19] K. Morimoto, M. Kato, M. Ogasawara, M. Kashimura, J. Nucl. Mater. 374 (2008) 378–385.
[20] R.E. Woodley, R.L. Gibby, Hanford Engineering Development Lab. Report, 1973. HEDL-SA-592, CONF-731041–6.
[21] R. Eichler, D. Hanus, J. Krellmann, R. Löb, H. Roepenack, J. Nucl. Mater. 124 (1984) 9–13.
[22] C. Guéneau, N. Dupin, B. Sundman, C. Martial, J.C. Dumas, S. Gossé, S. Chatain, F. De Bruycker, D. Manara, R.J.M. Konings, J. Nucl. Mater. 419 (2011) 145–167.
[23] H.L. Lukas, S.G. Fries, B. Sundman, Comp. Thermo., the Calphad Method, Cambridge Univ. Press, 2007.
[24] B. Sundman, B. Jansson, J.O. Andersson, Calphad 9 (1985) 153–199.
[25] T.M. Besmann, T.B. Lindemer, Oak Ridge Technical Report, 1984. CONF-841105–59.
[26] T.M. Besmann, T.B. Lindemer, J. Nucl. Mater. 130 (1985) 489–504.
[27] T.M. Besmann, T.B. Lindemer, Oak Ridge Technical Report, 1985. CONF-851115–34.
[28] R. Vauchy, A.C. Robisson, F. Audubert, F. Hodaj, Ceram. Inter 40 (7B) (2014) 10991–10999.
[29] R. Vauchy, A.C. Robisson, P.M. Martin, R.C. Belin, L. Aufore, A.C. Scheinost, F. Hodaj, J. Nucl. Mater. 456 (2015) 115–119.
[30] B. Ravel, M. Newville, J. Synchrotron. Radia 12 (2005) 537–541.
[31] K.O. Kvashnina, Y.O. Kvashnin, S.M. Butorin, J. Electron Spectrosc. Relat. Phenom. 194 (2014) 27–36.
[32] R. Böhler, M.J. Welland, D. Prieur, P. Cakir, T. Vitova, T. Pruessmann, I. Pidchenko, C. Hennig, C. Guéneau, R.J.M. Konings, D. Manara, J. Nucl. Mater. 448 (2014) 330–339.
[33] S.D. Conradson, B.D. Begg, D.L. Clark, C. den Auwer, M. Ding, P.K. Dorhout, F.J. Espinosa-Faller, P.L. Gordon, R.G. Haire, N.J. Hess, R.F. Hess, D. Webster Keogh, G.H. Lander, D. Manara, L.A. Morales, M.P. Neu, P. Paviet-Hartmann, J. Rebizant, V.V. Rondinella, W. Runde, C. Drew Tait, D. Kirk Veirs, P.M. Villella, F. Wastin, J. Solid State Chem. 178 (2005) 521–535.
[34] P.M. Martin, S. Grandjean, M. Ripert, M. Freyss, P. Blanc, T. Petit, J. Nucl. Mater. 320 (2003) 138–141.
[35] R.C. Belin, P.M. Martin, J. Léchelle, M. Reynaud, A.C. Scheinost, Inorg. Chem. 52 (6) (2013) 2966–2972.
[36] G.S. Pawley, J. Appl. Crystallogr. 14 (1981) 357.
[37] H.M. Rietveld, J. Appl. Crystallogr. 2 (1969) 65–71.
[38] M. Chollet, R.C. Belin, J.C. Richaud, M. Reynaud, F. Adenot, Inorg. Chem. 52 (5) (2013), 2519–1525.
[39] T. Ohmichi, S. Fukushima, A. Maeda, H. Watanabe, J. Nucl. Mater. 102 (1981) 40–46.
[40] R. Verma, P.R. Roy, Bull. Mater. Sci. 8 (4) (1986) 479–488.